International Journal of Engineering Research & Management Technology
(Peer-Reviewed, Open Access, Fully Refereed International Journal) ISSN: 2348-4039
Volume 12, Issue-1 January-February- 2025 Impact Factor: 7.09
Email: editor@ijermt.org www.ijermt.org

INVESTIGATION OF DIELECTRIC PROPERTIES OF RARE EARTH-DOPED PBTIO3 FOR ADVANCED ELECTRONIC APPLICATIONS

Shraddha Yadav
Research scholar
Sage university indore
Dr. Rajesh Kumar katare
Professor sage university Indore

ABSTRACT

Research into the dielectric characteristics of PbTiO3 that has been doped with rare earth elements has shown significant improvements in performance for advanced electrical applications. Research has shown that the phase transition properties and dielectric constant of lead titanate ceramics may be modified by doping them with rare earth elements such as Y, Pr, and Nd. Consider PbTiO3 that has been doped with Nd. The correlated barrier hopping idea takes into consideration the dielectric constants of the material and its frequency-dependent conductivity. It also explains why the material's dielectric behaviour is enhanced. Another example is the impact of co-doping praseodymium and yttrium on ferroelectric characteristics at ambient temperature. This is shown by an increase in piezoelectric coefficients and residual polarisation. The Correlated Barrier Hoping (CBH) model has been utilised to confirm the empirical findings of MPB. The relationship between the density of states of the conductance process and the behaviour of dielectric relaxation has been shown via the use of statistical theory, the quantum mechanical anharmonic oscillator model, and Jahn-Teller phenomena. This study examines a number of important elements, including as the density of states, the minimum hopping length, the dielectric constant, and the electrical conduction mechanism, as they relate to the temperature at which sintering occurs.

KEYWORD: dielectric, Rare Earth, Electronic

1. Introduction

Infrared (IR) sensors [1], micro-electromechanical systems (MEMS) [2], non-volatile memory [3], and ferroelectric thin films based on PbTiO3 (PT) are all used in a variety of technological applications. Furthermore, these films have distinct ferroelectric and piezoelectric properties. By adding the right amount of doping, it is possible to customise the dielectric and pyroelectric characteristics of the films for a given application. According to the literature review, La [4-12] has been the subject of more research than any other doping ingredient. Most of the systematic research that have been conducted on the behaviour of other elements in the lanthanide series have focused on bulk ceramic media. Park et al. [13] developed and studied PLZT (lead lanthanum zirconate titanate) ceramics that included 3 mol% of La, Nd, Sm, Gd, Dy, Ho, Er, and Yb, which are collectively referred to as Ln. Tan et al. [14] and Sharma et al. [15] described the structure and characteristics of PZT (lead zirconate titanate) ceramics in relation to the ionic radii of rare-earth elements. Pramila et al. [16] and provided a thorough description of the properties of PZT ceramics that were treated with La, Sm, and Er. Researching the dielectric properties of PbTiO3 that has been doped with rare earth elements for application in advanced electronics gives us new insights into how doping affects the structural and functional properties of materials. Researchers have investigated the interaction between PbTiO3 and rare earth elements.

REVIEW OF THE LITARTURE

Tomohiro Abe; Sangwook Kim ; Chikako Moriyoshi ; Yuuki Kitanaka ; Yuji Noguchi ; Hiroshi Tanaka; Yoshihiro Kuroiwa (2020)[17] This study used the Rietveld and maximum entropy methodologies to analyse synchrotron-radiation powder x-ray diffraction (SXRD) data in order to effectively display the valence electron density distributions of the ferroelectrics PbTiO3 and BaTiO3. The polarisation of the Pb ion in PbTiO3 in the ferroelectric phase is evident from the SXRD data. This is in contrast to BaTiO3, where the Ba ion is completely ionised as Ba2+. The Pb ion is highly electrically polarised because of the anisotropic spatial distribution of the

lone-pair electrons in the Pb2+ ion. This is especially true in the anisotropic p-like orbital that arises when Pb-O covalent bonds are created. The spontaneous polarisation in PbTiO3 is mostly determined by the electronic polarisation of the Pb ion. We show that the spontaneous polarisation can be derived from the SXRD data as the sum of the ionic and electronic polarisations, respectively, by empirically evaluating their contributions from the valence electron density distribution map. As the phase transitions, PbTiO3 breaks a Ti-O covalent link, but BaTiO3 keeps its atomic coordination intact. We suggest layered materials that include PbTiO3 in the ferroelectric phase and that take care of the covalent bonding network. This is confirmed by the findings of the first-principles calculations. We would want to combine SXRD testing with first-principles calculations in order to undertake more thorough investigations of valence electron density. This would help us to better understand the origins of ferroelectricity.

Shun, Zhou., Dabin, Lin., Yongming, Su., Lin, Zhang., Weiguo, Liu. (2021).[18] This study looks closely at the phase structure, electrical characteristics, and photoluminescence performance of thin ferroelectric films utilising compositions near the morphotropic phase boundary.

S., Yakovlev., C.-H., Solterbeck., Eivind, Morten, Skou., Mohammed, Es-Souni. (2006).[19] This study investigates the structural characteristics of Er-doped lead titanate thin films. Atomic force microscopy, X-ray diffractometry, and micro-Raman spectroscopy are among the techniques used in this study. The results indicate that the tetragonality factor, the c/a ratio, the E(1TO) transverse optical phonon frequency, the grain size, and the transition from the ferroelectric to the paraelectric phase are all impacted by the Er doping.

Karan, Singh., Vishal, Singh., Rashmi, Gupta., K., K., Bamzai. (2014) [20] This research presents four lead titanate compositions that include equal amounts of praseodymium and yttrium. The basic formula for these compositions is Pb1-xPrxTi1-yYyO3. In this case, x (praseodymium) and y (yttrium) are equal to 0.02, 0.04, 0.06, and 0.08.

Haiying, Xing., Chao, Yan., Qingwei, Liao., Lei, Qin., Chao, Zhong. (2017).[21] Researchers looked at the possibility of using PbTiO3 ceramics modified with LiYW2O8, a material that has chiral symmetry, as high-frequency transducers or actuators. The findings of the densification test indicate that the LiYW2O8 modified PbTiO3 ceramics have excellent sintering capabilities at a temperature of 900 °C. The piezoelectric constant is closely connected to the difference in time between polarisation and unpolarization relaxation. The dipole relaxation of PbTiO3 ceramics occurred at about 107 Hz. Tetragonality is closely connected to d33, K33, and Np. While d33, K33, and Tetragonality are all bigger, Np is smaller. The PbTiO3-0.35wt.% LiYW2O8 ceramic satisfies the criteria for high frequency transducers with a d33 of 68 pC/N and a K33 of 245.4.

A.K., Katna., R.K., Kotnala., Nainjeet, Singh, Negi. (2013).[22] In this work, lead titanate nanoparticles containing 1-4 percent Ni were synthesised by annealing them for three hours at a temperature of 700 degrees Celsius, following the fundamental metallo-organic decomposition (MOD) process.

OBJECTIVE OF THE STUDY

1. To Examining Rare Earth-Doped PbTiO3's Dielectric Properties for Cutting-Edge Electronic Applications
2. To look at things like the electrical conduction mechanism, density of states, minimum hopping length, and dielectric constant.

Experimental

Lead titanate (PT) and neodymium-modified lead titanate (PT) are two nanoceramics that have the same formula. The compounds Pb1-3x/2NdxTiO3 and PbTiO3 were synthesised using TiO2 provided by Merck and PbO, Nd2O3, and TiO2 supplied by Sigma-Aldrich, which had a purity of 99.9%. X was given a value of 0.01. At the beginning, a stoichiometric ratio was utilised to mix the unpurified oxides. According to my research, the ZnO hollow nanospheres that were formed might potentially be utilised to manufacture optoelectronic devices.

Additionally, this provides the general recipe for creating the compound. Molecules on the nanoscale might perhaps be

$$2\left(1-\frac{3x}{2}\right)PbO + 2TiO_2 + xNd_2O_3 \rightarrow 2Pb_{1-\frac{3x}{2}}Nd_xTiO_3 \quad (1)$$

There are many methods that have been developed to reduce the temperature at which phase formation occurs. These methods include the chemical vapour method, the sol-gel technique, the hydrothermal method, the solid-state reaction method, and molten salt synthesis. However, each of these strategies has its own advantages and disadvantages. High energy ball milling (HEBM) is a method that may be used to synthesise compounds in a simple and inexpensive way.

Lead titanate is still a commonly used host material since it has the ability to improve the dielectric constant, even if researchers are trying to create ceramics that do not include lead in order to address environmental issues. Optoelectronics and the creation of sensors and actuators are only a few of the numerous potential uses for it. These days, a common method for improving the performance of a base molecule is to add rare earth ions to it. The HEBM method may be used to successfully create nano-crystalline ceramics and a variety of alloys [23-25]. As far as we know, this is the first publication to explore the use of HEBM for the fabrication of nanocrystalline ceramics of PT doped with Nd. Earlier work on PT doped with Gd was published by Parasar et al. [26]. Researchers have studied the dielectric and electrical characteristics of nanocrystalline PNT ceramics. The conduction method of charge transport in the system has been identified using impedance spectroscopy characteristics and conductivity data [27, 28]. The findings from the field may be confirmed using the Correlated Barrier Hoping (CBH) model.

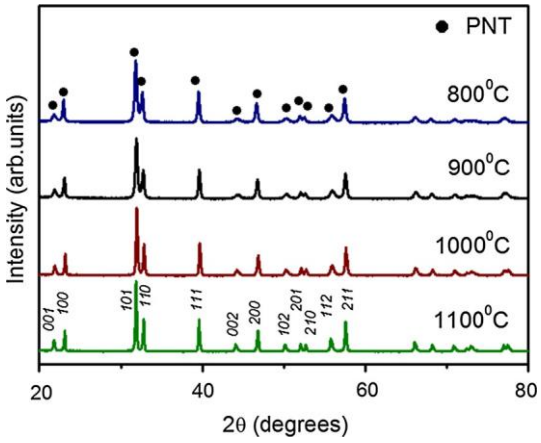
PNT synthesis was accomplished using high

A ball milling method that makes use of energy Planetary ball milling was performed at room temperature for lengths of time ranging from zero to twenty hours. The equipment used for this process was a Retsch PM 200 planetary ball mill, which was produced by Retsch in Germany. The milling technique included the use of a tungsten carbide (WC) vial and WC balls that were 10 mm in diameter. The balls-to-powder weight ratio was 20:1, and the speed was 300 rpm. The samples were sintered in an air environment at a temperature of 800 °C for a duration of two hours. Before any measurements were performed, the sintered pellets were first coated with Alpha Aesar, a high-purity silver paste, which gave them their smooth, polished surfaces. After 15 minutes of drying at 700 °C, the surfaces may be ready for evaluation. The same method was utilised to sinter more ceramic pellets at temperatures of 900, 1000, and 1100 °C. The electrical parameters were measured using an HIOKI-3532 LCR Hitester. The measurements were taken in a moderate electric field of around 1 V, at temperatures between 100 and 525 °C, at frequencies between 102 and 106 Hz, and at a heating rate of 4 °C/min.

Results and discussion

Structure and microstructure

The XRD pattern (k = 0.15418 nm) obtained using Cu Ka radiation is given in Fig. 1. The ceramics of PNT (Pb1-3x/2NdxTiO3) with x = 0.01 were sintered at temperatures ranging from 20° to 80° for 2 hours. The majority of the PNT peaks were located and indexed by use of tetragonal XRD spectra.



The XRD pattern of PNT (Pb1-3x/2NdxTiO3) ceramics, which has an x-value of 0.01, is illustrated in Figure 1. The X-pert high score plus optical system was used to carry out a 20-hour sintering operation on these ceramics at the following temperatures: a, 800 °C; b, 900 °C; c, 1000 °C; and d, 1100 °C. The PT ceramic has also been studied for similar patterns. The structural integrity of the prepared ceramics was maintained when they were sintered at various temperatures. According to new studies, stressors have a negative effect on the characteristics of materials [29, 30]. The tetragonality ratio (c/a) of the PNT ceramic that was sintered at 800 °C was determined to be 1.0443, and this ratio changes depending on the temperature at which the sintering process occurs. The reduction in porosity and the rise in grain boundary size are the reasons for this c/a ratio fluctuation. At 800 °C, the average crystallite size was 20.75 nm and the average lattice strain was 0.012, according to Scherrer's formula [31]. Table 1 contains data on the synthesised nanocrystallite lead titanate that has been doped with 1 mol% neodymium in the 'A' site of the perovskite structure at room temperature (RT) and sintered at various temperatures. Furthermore, the lattice parameters a and c (in A˚), the unit cell volume V (in A˚)3, the average crystallite size P (in nm), and the lattice strain estimated from XRD experiments using POWD software [32] may all be found.

Dielectric investigations and SEM micrographs

The findings of a SEM study of PNT ceramic microstructures that were sintered at various temperatures are shown in Figure 2. The two parameters are positively correlated because, as the sintering temperature rises, the size of the grains reduces and the porosity increases. Sintering is a procedure that employs mechanical pressure or heat to create a solid mass from a liquid that has not melted. When the atoms of a material extend beyond the boundaries of its particles and fuse them together, a solid is produced. Sintering is a typical technique for shaping materials with high melting points since the process temperature remains below the melting point of the material. Sintering is a process that uses heat energy to create grain boundaries that develop across pores, resulting in denser material. Grain growth is controlled by the repositioning of the grain boundary and the interlocking of larger and smaller crystal grains [33, 34].

This image makes it evident that although the particle distributions are not uniform, agglomeration rises as the sintering temperature rises.

Researchers have changed the temperature from 100 to 525 °C in order to find out the dielectric constant of PT and PNT ceramics at various frequencies. Figure 3 shows the dielectric constant for PT ceramics at different temperatures, whereas Figure 4 shows the same data for PNT ceramics at 1, 10, 100 kHz, and 1 MHz. The graphs of the sample demonstrate that the dielectric constant (er) reaches its highest point when it goes through a phase transition from ferroelectric to paraelectric. The dielectric constant of the ceramic material is at its greatest for all observed frequencies when the temperature is at 470 °C, which is the curie temperature of the ceramic material. The difference between the two sets of graphs demonstrates that PNT has a greater dielectric constant than undoped PT. The rise in PNT dielectric constant values confirms that Nd is present in the host perovskite

structure. Several studies [35–36] have shown the consequences of partially substituting Pb2+ ions at the A-site with Ca2+, Sr2+, or La3+ ions. It has been reported that the static average electric dipole polarisability value of Pb is 6.8 × 10-24 cm3, whereas the value for Nd is 31.4 × 10-24 cm3 [37-39]. This kind of ceramic is made from materials that have a high dielectric constant at low frequencies. The atomic dipoles' inclination to follow the field at low frequencies is what causes this. Ionic polarisability, unit cell volume V, crystal structure (CS), lattice parameters (a and c in A˚), nanocrystallite perovskite lead neodymium titanate (PNT) lattice strain, and average crystallite size (P in nanometres) are all most pronounced in the low frequency region, according to Table 1."

System	Temperature (℃)	CS	a (Å)	c (Å)	c/a	V (Å)^3	P (nm)	Strain
PNT	Room temperature	Tetragonal	3.8867	4.0717	1.0476	61.51	20.75	0.012
	800	Tetragonal	3.8773	4.0378	1.0414	60.70	10.86	0.0258
	900	Tetragonal	3.8792	4.0563	1.0475	60.83	27.49	0.0093
	1000	Tetragonal	3.8725	4.0589	1.0463	61.08	21.95	0.0102
	1100	Tetragonal	3.8767	4.0739	1.0509	61.22	37.48	0.0049

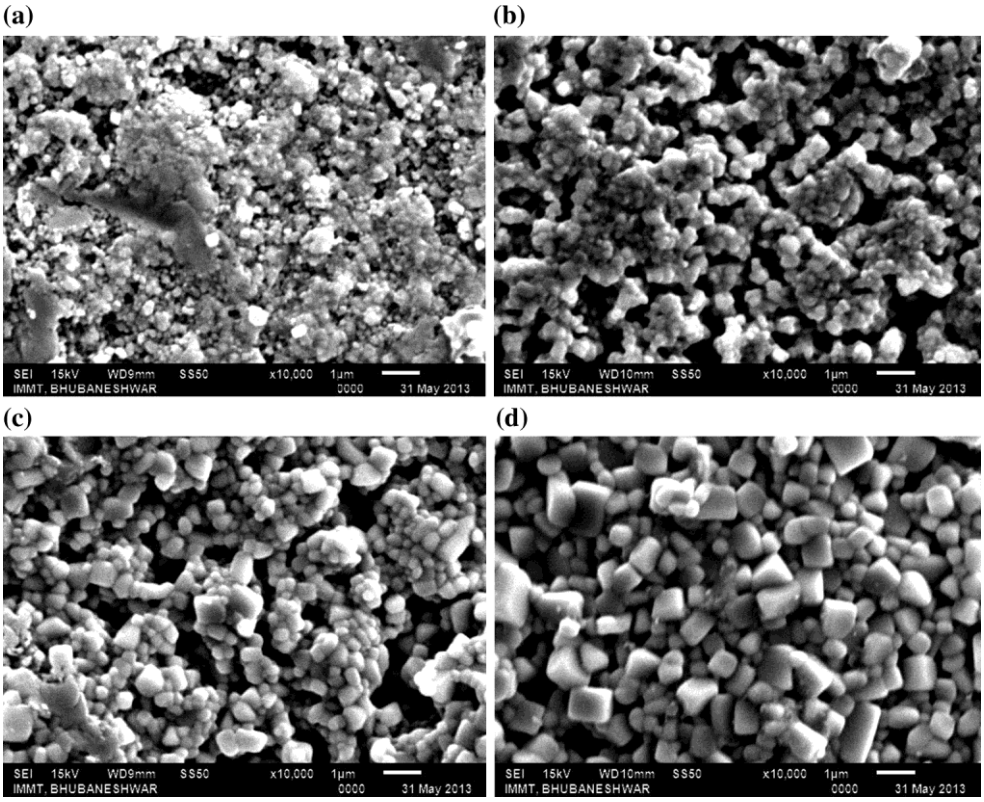


Fig. 2 SEM micrographs of PNT sintered at 800, 900, 1000, and 1100 degrees Celsius

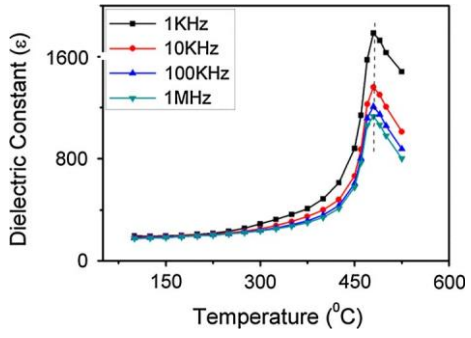


Fig. 3 Dielectric constant temperature dependency for PT ceramics sintered at 800 °C at 1, 10, 100 kHz, and 1 MHz

The primary topic of [40–42] is electronic polarisability. All of the samples show dielectric dispersion with frequency at lower frequencies. Koop's phenomenological hypothesis [43–45] and an explanation that is based on Maxwell-Wagner type interface polarisation are two possible explanations. Space charge polarisation, which is a result of an uneven dielectric structure, is the reason why the dielectric constant value is large at low frequencies. The present system's lack of homogeneity is caused by a combination of contaminants, porosity, and grain structure. When the sintering temperature is increased, the density also increases, which causes the electrical resistance to decrease and the dielectric constant to increase.

Density of states

Figure 5 shows the results of the research about the density of states as a function of frequency and temperature. The image clearly shows that the density of states grows with temperature everywhere up to the MPB, but thereafter it begins to drop. It seems that there is a distribution of free time based on the dispersion behaviour. The significance of a temperature-dependent relaxation mechanism in the base molecule cannot be overstated. As low-frequency temperatures increase, the density of states also rises. An increase in CBH is thought to be the cause of this. The density of states decreases as the frequency increases because of the larger time lag between the applied field and the atomic dipole. As the sintering temperature increases, the density of states also increases due to the grain size (Table 1) and the base compound's decreasing porosity and growing density (Fig. 2).

Conduction mechanism

Hopping, quantum tunnelling, and trapping centres will probably have a significant impact on AC conductivity in disordered materials. Localised states allow for the representation of the AC electrical conductivity in most materials as [46].

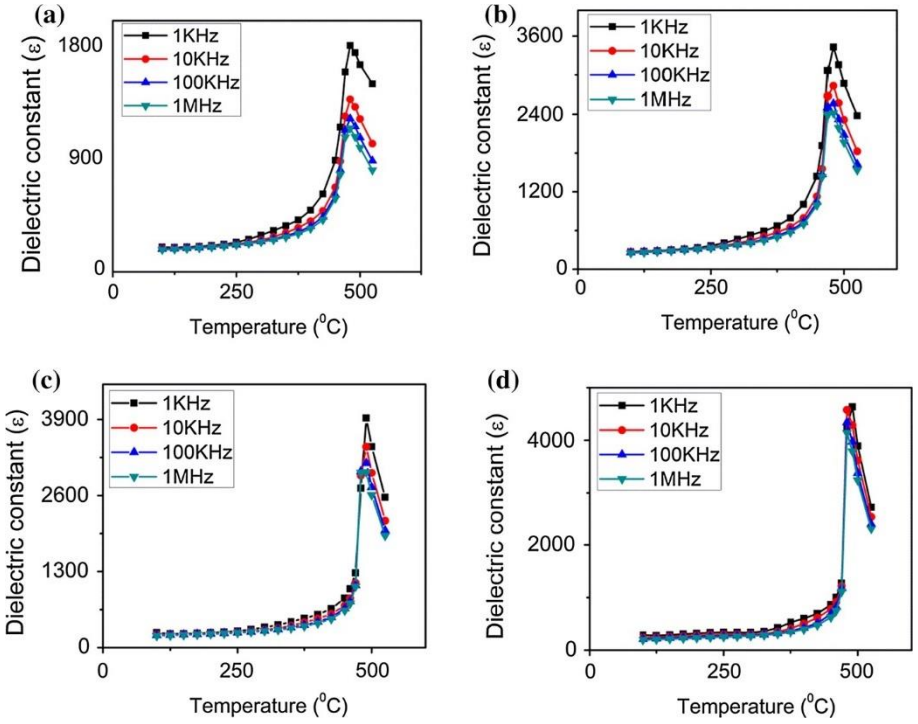


Fig. 4 Temperature dependence of dielectric constant for PNT ceramics sintered at 800°C, 900°C, 1000°C, and 1100°C at 1, 10, 100 kHz, and 1 MHz

$$\sigma'(\omega) = \sigma_0 + A\omega^s \quad (1)$$

The frequency-independent (electronic or DC) component of AC conductivity is denoted by 'σ0' in this context, the index by's(0≤ s < 1)', the angular frequency of the applied AC field by 'x', a constant by A = πN2e2 /6KBT(2α), the electronic charge by 'e', "T" stands for temperature. 'N' is the number of sites per unit volume where hopping takes place, and 'a' is the polarisability of two sites. The word "Axs" in carrier conduction may be explained utilising both quantum mechanical tunnelling (QMT) and correlated barrier hopping (CBH) across the barrier that divides the localised sites. These models show two different patterns of exponent-dependent temperature and frequency. The temperature does not affect the variables in QMT, and it is expected that the temperature will drop as 'ü' increases.

$$s = 1 + \frac{4}{\log(\omega\tau_0)} \quad (2)$$

'$\tau 0$' is the typical amount of time spent relaxing. The expression for the AC conductivity is [47]

$$\sigma' = \frac{\pi^4}{24} e^2 \omega K_B T [N(E_F)]^2 \alpha^{-1} R_\omega^4 \quad (3)$$

where 'α^{-1} ' is the localised wave function's spatial decay parameter, and '$R\omega$' is the length of the tunnel at frequency 'ω' and may be stated as,

$$R_\omega = \frac{1}{2\alpha} \ln\left(\frac{1}{\omega\tau_0}\right)$$

Additionally, if AC conductivity originates from CBH [48], then

$$\sigma' = \frac{\pi}{3} e^2 \omega K_B T [N(E_F)]^2 \alpha^{-5} \left[\ln\left(\frac{f_0}{\omega}\right)\right]^4 \quad (4)$$

The localised wave function is represented by the letter "a," the photon frequency is represented by the letter "f0," and the density of states at the Fermi level is represented by the letter "#N(EF)". The exponent's may be represented in another way: [49],

$$s = 1 - \frac{6K_B T}{W_m} \quad (5)$$

The amount of energy required to transport one electron from one location to another is termed the binding energy, and it is abbreviated as "Wm."

Figure 6 illustrates the connection between and the temperature. As shown in the figure [Eq. (1)], the near-zero behaviour of s at higher temperatures and its atypical temperature dependence suggest that DC conductivity is the dominant factor in the low frequency zone at these temperatures. The experimental results show that CBH may be found in PT and PNT ceramics.

Consequently, short-range translational charge carrier hopping may be the source of conduction in the system. The curve's slope shifts after the MPB, as seen in Figure 6, suggesting that the conduction mechanism becomes temperature-dependent.

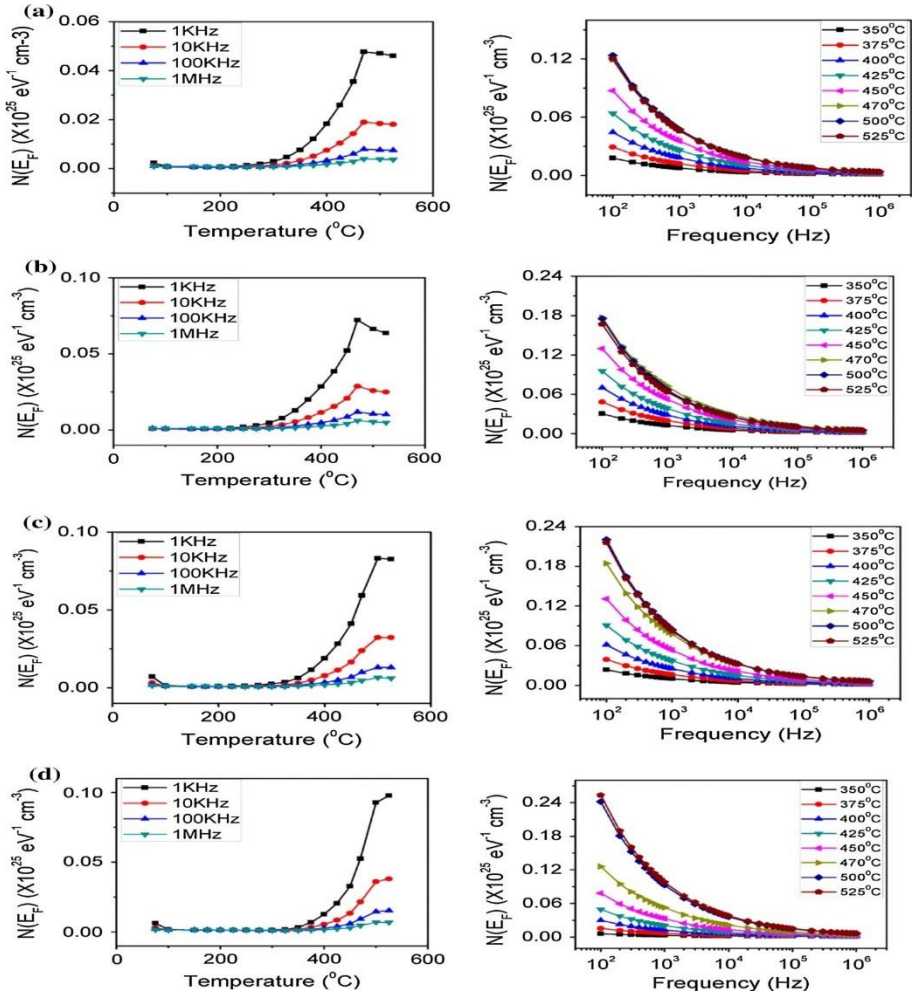


Fig. 5 Frequency (HZ) and temperature (°C) density of states [N(EF)] dependency for PNT ceramics sintered at 800, 900, 1000, d, and 1100 degrees Celsius

about the temperature and frequency fronts. The Nd-doped host also has semiconductor-like features, including a negative temperature coefficient of resistance, since the ac conductivity values fall as the temperature increases following MPB. One possible explanation for this might be the activation of charge species at grain boundaries as a result of heat. According to the experimental findings of this work, a charge conduction mechanism is activated by heat [50].

A charge carrier may hop from one location to another over the shortest distance feasible (the minimum hopping length) by [49, 51],

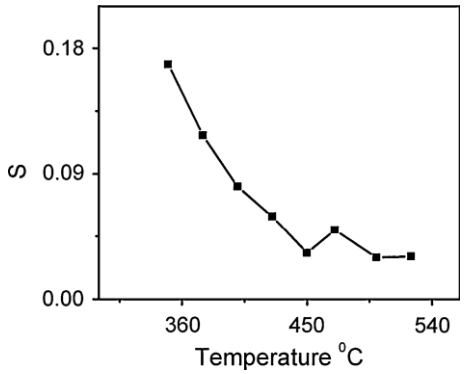


Fig. 6 Temperature dependency of the AC electrical conductivity index factor "s"

$$R_{\min} = \frac{2e^2}{\pi\varepsilon\varepsilon_0 W_m} \quad (6)$$

The definitions of the terminology used here are the same as they are in most cases. Figure 7 shows the temperature-vs-minimum hopping-length plot, which was created using the graph of the dielectric constant against temperature (Fig. 3) and Equation 6. The findings clearly show that the minimum hopping time becomes shorter as the sintering temperature rises. This might be due to the fact that PNT ceramics have a lower porosity and smaller granules. For all sintering temperatures, the minimal Rmin value is reached at MPB. As seen in Figure 7, the time it takes to reach the lowest hopping length grows as the frequency increases. Atomic dipoles are a product of polarisation. They follow the applied field at low frequencies, but at higher frequencies, they start to lag behind. At low frequencies, ionic and dipolar polarizabilities are the most important, while at high frequencies, the effect of electronic contribution becomes more noticeable. The host's temperature-sensitive relaxation mechanism might be responsible for the considerable increase in Rmin.

Theoretical interpretation

This research, like earlier studies on CBH, employs experimental approaches to investigate how the distribution of electron density varies between lead and oxygen. The hybridisation of (Ti-3d) and (O-2p) together with the temperature-dependent bonding of (Pb-O) is one of the most important factors that influence the ferroelectric stability of PT compounds, according to theoretical research [52-54]. Covalent bonding is frequent in (Pb-O), however when the temperature rises, the electron clouds shift and the charges move virtually as if they were stationary. The dielectric constant rises and the displacement of charges decreases when an electric field is applied [55, 56]. The dielectric constant of the medium between the conducting plates is affected by increases in the potential difference between the plates in the same way that it is affected in a parallel plate capacitor. The Jahn-Teller effect may provide some insight into the hybridisation process of (O-2p) and (Ti-3d). This event happened because

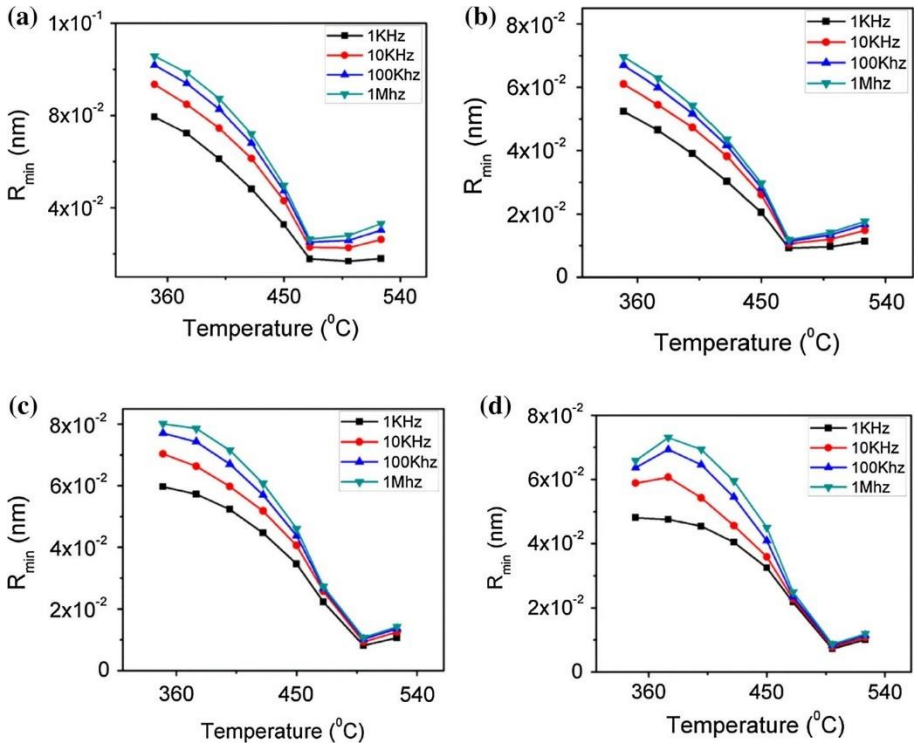


Fig. 7 For PNT ceramics sintered at a, 800 °C, b, 900 °C, c, 1000 °C, and d, 1100 °C, the minimum hopping duration at 1, 10, 100 kHz, and 1 MHz vs temperature

Change from a cubic phase to a tetragonal phase. The CBH model also accurately predicts how the MPB will affect the behaviour of the hopping conduction mechanism.

The Ti ion weakly connects the octahedron cage, which is made up of six oxygen atoms in each unit cell of PbTiO3, to the core. In these perovskite systems, the local electric field that is produced by the titanium ions in the crystal is stronger than the elastic restoring forces. The Ti ion in the crystal produces a harmonic oscillator that has harmonic phrases. This results in an unequal shift in the equilibrium position and the creation of a dipole moment [53]. The situation gets more complicated since the bonding between lead and oxygen molecules is influenced by both temperature and polarity in the current host. John Barrett has previously calculated the dielectric constant of barium titanate, which is similar to lead titanate, using a quantum mechanical approach that is similar to a three-dimensional anharmonic oscillator. This calculation was done with the addition of a first-order correction to the energy, since the system is disturbed in the end [57]. The polarisation catastrophe might be used to find out whether the disruption is possible. While barium titanate has the same characteristic, the lead-oxygen connection is what sets lead titanate apart from barium titanate.

This represents the system's induced net ionic polarisability.: [57]

$$\alpha'_{T_i} = \frac{q^2}{2a}\left[1 - \left\{(3b_1 + 2b_2)\frac{hv}{2a^2}\right\}\coth\left(\frac{hv}{2kT}\right)\right] \quad (7)$$

where every term has a standard definition [48]. The following is the equation for the dielectric constant ε that is linked to polarisability:

$$\varepsilon = A + \frac{B}{(1 - D\chi'_{T_i})} \quad (8)$$

, where the values of A, B, and D do not change. The electronic polarizabilities of particular atoms and the geometrical arrangements of the perovskite crystal are used to establish the values of constants A, B, and D.and

$$\chi'_{T_i} = \frac{\alpha'_{T_i}}{\varepsilon_0 V} \quad (9)$$

The letter V represents the volume of the unit cell. If hυ is equal to kT during the paraelectric phase, then it is possible to keep Eq. (7). According to the trigonometric function in Eq. (7), which has the limitation hυ kT, α' Ti decreases as the temperature increases along with a change in phase transition. This is the reason why the dielectric constant of all PNT ceramics that have been sintered at different temperatures and frequencies decreases significantly at 470 C, which is also known as the Curie temperature or the MPB transition temperature.

Eq. (8) may be changed by using the differentiation mathematical techniques as $\frac{d\varepsilon}{dT} = \frac{BD}{(1-D\chi_{T_i})^2}\left\{\frac{d\chi_{T_i}}{dT}\right\}$, $\frac{d\chi_{T_i}}{dT}$

decreases as the temperature rises, and then decreases again. Mott's idea suggests that the likelihood of moving from one condition to another that are separated by space (R) and energy (E) may be stated as [68].

$$P(R,E) = \exp\left[-2\alpha R - \frac{E}{kT}\right] \quad (10)$$

Eq. (10) may be expressed as follows using the Taylor series expansion:

$$P(R,E) = P(R_0,E_0) + (R-R_0)\frac{\partial P}{\partial R}|_{R_0,E_0} + (E-E_0)\frac{\partial P}{\partial E}|_{R_0,E_0} + \frac{1}{2}\left[(R-R_0)^2\frac{\partial^2 P}{\partial R^2}|_{R_0,E_0} + (E-E_0)^2\frac{\partial^2 P}{\partial E^2}|_{R_0,E_0} + \cdots\right] \quad (11)$$

Limiting the expansion to words of the first order

$$P(R,E) = \exp\left[-2\alpha R_0 - \frac{E_0}{kT_0}\right] + \left\{(R-R_0)e^{\frac{-E_0}{kT_0}}.e^{-2\alpha R_0}(-2\alpha) + (E-E_0)e^{\frac{-E_0}{kT_0}}.e^{-2\alpha R_0}\left(-\frac{1}{kT_0}\right)\right. \quad (13)$$

When T is greater than TC, we say that the temperature is critical at MPB. When the dipole separation grows, the atomic dipoles get disoriented in the domain where ΔT approaches 0 following the MPB. As a result, the density of states and the dielectric constant are decreased since it is less probable that electron conduction will take place (Figs. 4, 5).

Conclusion

We employed HEBM to sinter nanocrystalline PT and PNT ceramics with tetragonal architectures at various temperatures. Then, we employed XRD and SEM to characterise them. As the sintering temperature and neodymium incorporation rise, the peak value of the dielectric constant and the density of states also increase. This is due to the fact that the grain boundary's size and porosity are decreased. After the MPB, the dielectric constant and density of

states values at all frequencies drop sharply, which suggests that there is a transition from the ferroelectric state to the paraelectric state. The conduction mechanism in PNT is thought to function because of the increased likelihood of electrical conduction that is caused by CBH. The dielectric constant, density of states, and minimum hopping length curves all exhibit a dispersion in their behaviour, which indicates that the material's relaxing process is sensitive to temperature. The experimental evidence supports the mathematical hypothesis that was presented by John Barrett. This research shows that nanocrystallite PNT ceramics might be a promising material for a variety of microelectronic devices, such as memory devices, in the future.

References

1. D.L. Polla and L.F. Francis, MRS Bull., 21, 59 (1996).
2. R. Ramesh, S. Aggarwal, and O. Auciello, Mater. Sci. Eng., 32, 191 (2001).
3. W. Wersing and R. Bruchhaus, in Handbook of Thin Film De-vices, edited by M.H. Francombe (Academic Press, New York, 2000), vol. 5, p. 168.
4. S.B. Lang and D.K. Das-Gupta, in Handbook of Advanced Elec-tronic and Photonic Materials and Devices, edited by H.S. Nalwa (Academic Press, San Diego, 2001), vol. 4, p. 22.
5. M. Alguero, M.L. Calzada, and L. Pardo, J. Mater. Res., 14, 4570 (1999).
6. M. Alguero, M.L. Calzada, and L. Pardo, J. Eur. Ceram. Soc., 19, 1481 (1999).
7. S.J. Kang, J.S. Ryoo, and Y.S. Yoon, in Ferroelectric Thin Films IV, edited by B.A. Tuttle, S.B. Desu, R. Ramesh, and T. Shiosaki (Materials Research Society, Pittsburgh, 1995), vol. 361, p. 281.
8. T. Kamada, R. Takayama, A. Tomozawa, S. Fujii, K. Iijima, and T. Hirao, in Ferroelectric Thin Fims V, edited by S.B. Desu, R. Ramesh, B.A. Tuttle, R.E. Jones, and I.K. Yoo (Materials Research Society, Pittsburgh, 1996), vol. 433, p. 377.
9. Y.-K. Tseng, K.-S. Liu, J.-D. Jiang, and I.-N. Lin, Appl. Phys. Lett., 72, 3285 (1998).
10. Y.M. Kang, J.K. Ku, and S. Baik, J. Appl. Phys., 78, 2601 (1995).
11. M. Es-Souni, M. Abed, A. Piorra, S. Malinowski, and V. Zaporojtchenko, Thin Solid Films, 389, 99 (2001).
12. H.-B. Park, C.Y. Park, Y.-S. Hong, K. Kim, and S.-J. Kim, J. Am. Ceram. Soc., 82, 94 (1998).
13. Q. Tan, Z. Xu, and D. Viehland, Phyl. Mag. B, 80, 1585 (2000).
14. H.D. Sharma, A. Govindan, T.C. Goel, P.K.C. Pillai, and C. Pramila, J. Mater. Sci. Lett., 15, 1424 (1996).
15. C. Pramila, T.C. Goel, and P.K.C. Pillai, J. Mater. Sci. Lett., 12, 1657 (1993).
16. S.R. Shannigrahi, R.N.P. Choudhary, and H.N. Achatya, Mater. Res. Bull., 34, 1875 (1999).
17. **Tomohiro Abe; Sangwook Kim ; Chikako Moriyoshi ; Yuuki Kitanaka ; Yuji Noguchi ; Hiroshi Tanaka; Yoshihiro Kuroiwa (2020) Visualization of spontaneous electronic polarization in Pb ion of ferroelectric $PbTiO_3$ by synchrotron-radiation x-ray diffraction,** AIP Journal, **Volume 117, Issue 25, https://doi.org/10.1063/5.0037396.**
18. S., Yakovlev., C.-H., Solterbeck., Eivind, Morten, Skou., Mohammed, Es-Souni. (2006). Structural and dielectric properties of Er substituted sol-gel fabricated PbTiO3 thin films. Applied Physics A, 82(4):727-731. doi: 10.1007/S00339-005-3444-5
19. Karan, Singh., Vishal, Singh., Rashmi, Gupta., K., K., Bamzai. (2014). Structural, dielectric, piezoelectric and ferroelectric behavior of rare earth double doped lead titanate ceramics synthesized by solid state method. IOSR Journal of Applied Physics, 6(4):08-14. doi: 10.9790/4861-06410814
20. Haiying, Xing., Chao, Yan., Qingwei, Liao., Lei, Qin., Chao, Zhong. (2017). Dielectric polarization and electrical properties of Modified PbTiO 3 Piezoelectric Ceramics for high frequency transducer applications. 94(1):012081-. doi: 10.1088/1755-1315/941/012081
21. A.K., Katna., R.K., Kotnala., Nainjeet, Singh, Negi. (2013). Acceptor dependent structural, microstructural and dielectric properties of PbTiO3 nano-particles. Physica B-condensed Matter, 425:95-99. doi: 10.1016/J.PHYSB.2013.05.024

22. Shun, Zhou., Dabin, Lin., Yongming, Su., Lin, Zhang., Weiguo, Liu. (2021). Enhanced dielectric, ferroelectric, and optical properties in rare earth elements doped PMN-PT thin films. Journal of Advanced Ceramics, 10(1):98-107. doi: 10.1007/S40145-020-0423-4
23. S.K.S. Parasar, R.N.P. Choudhary, B.S. Murty, J. Appl. Phys. 94, 6091 (2003)
24. D.J. Fatemi, V.G. Harris, V.H. Browning, J.P. Kiekland, J. Appl. Phys. 83, 6867 (1998)
25. L.B. Kong, J.M. Zhu, W.T. OK, J. Alloys Compd. 236, 242 (2002)
26. S.K.S. Parasar, S. Chaudhuri, S.N. Singh, M. Ghoranneviss, J. Theor. Appl. Phys. 7, 26 (2013)
27. K. Prabhakar, S.P. Mallikarjun Rao, J. Alloys Compd. 437, 302 (2007)
28. S.K. Rout, A. Hussain, J.S. Lee, J.S. Lee, I.W. Kim, S.I. Woo, J. Alloys Compd. 477, 706 (2009)
29. A.Pramanick, J.L. Jones, G. Tutuncu, D. Ghosh, A.D. Stoica, K. An, Sci. Reports 2, 929 (2012)
30. F. Li, S. Zhang, Z. Xu, X. Wei, T.R. Shrout, Adv. Funct. Mater. 21, 2118 (2011)
31. C. Suryanarayana, Prog. Mater. Sci. 46, 1 (1998)
32. E. Wu, POWD, An Interactive Powder Diffraction Data Inter- pretation and Indexing Program, Version 2.1, School of Physical Science, Flinders, University of South Australia, Bedford Park, S.A., 5042, Australia
33. C. Barry Carter, M. Grant Norton, Ceramic Materials (Springer, New York, 2012)
34. R. Islam, Md Rahman, M.A. Hakim, D.K. Saha, S. Saiduzzaman,
35. S. Noor, Md Al-Mamun, Mater. Sci. Appl. 3, 1 (2012)
36. L.B. Kong, T.S. Zhang, J. Ma, F. Boey, Prog. Mater. Sci. 53, 207 (2008)
37. Y. Xu, Ferroelectric Materials and Their Applications (Elsevier, Amsterdam, 1991)
38. J. Portelles, N.S. Almodovar, J. Fuentes, O. Raymond, J. Heiras,
39. J.M. Siqueiros, J. Appl. Phys. 104, 73511 (2008)
40. K.D. Bonin, K. Kallen, Int. J. Mod. Phys. B 24, 3313 (1994)
41. T.M. Miller, B. Bederson, Adv. At. Mol. Phys. 13, 1 (1977)
42. H. Gould, T.M. Miller, Adv. At. Mol. Opt. Phys. 51, 243 (2005)
43. M.K. Gergs, G.A. Gamal, M.A. Massaud, Ceram. Egypt. J. Solid 30, 20 (2007)
44. M. Kellati, S. Sayouri, N. El Moudden, M. Elaatmani, A. Kaal, M. Taibi, Mater. Res. Bull. 39, 867 (2004)
45. Ravender Tickoo, R.P. Tandon, K.K. Bamzai, P.N. Kotru, Mater. Sci. Eng. B 103, 145 (2003)
46. J.C. Maxwell, Electricity and Magnetism (Oxford University Press, London, 1973)
47. K.W. Wagner, Ann. Phys. 40, 818 (1993)
48. C.G. Koops, Phys. Rev. 83, 121 (1951)
49. A.K. Jonscher, Nature 267, 673 (1977)
50. S.R. Elliott, Adv. Phys. 36, 135 (1987)
51. G.D. Sharma, M. Roy, M.S. Roy, Mater. Sci. Eng. B 104, 15 (2003)
52. S. Mollah, K.K. Som, K. Bose, B.K. Chaudhari, J. Appl. Phys. 74, 931 (1993)
53. J. Kumar, S.N. Choudhary, K. Prasad, R.N.P. Choudhary, Adv. Mater. Lett. 5, 106 (2014)
54. H. Miyazawa, E. Natori, S. Miyashita, T. Shimoda, F. Ishii, T. Oguchi, Jpn. J. Appl. Phys. 39, 5679 (2000)
55. S.R. de Lazaro, E. Longo, A. Beltran, J.R. Sambrano, Quim. Nova. 28, 10 (2005)
56. B. Ravel, E.A. Stern, J. Phys. IV France 7, C2–C1223 (1997)
57. R. Salam, Phys. State. Solid. A 117, 535 (1990)
58. E.A. Kotomin, Y.F. Zhukovskii, S. Piskunov, D.E. Ellis, J. Phys. 117, 012019 (2008)
59. S. Piskunov, E.A. Kotomin, E. Heifets, J. Maier, R.I. Eglitis, G. Borstel, Surf. Sci. 575, 75 (2005)
60. J.H. Barrett, Phys. Rev. 86, 1 (1952)
61. N.F. Mott, Philos. Mag. 19, 835 (1969)